SiO_2 precipitation in highly supersaturated oxygen-implanted single-crystal silicon

G. F. Cerofolini, S. Bertoni, P. Fumagalli,* L. Meda, and C. Spaggiari
Istituto Guido Donegani, Via Fauser 4, 28100 Novara NO, Italy
(Received 5 October 1992)

An extended transmission-electron-microscopy investigation of oxygen-implanted silicon has been carried out and has given evidence for a new precipitation mechanism. This mechanism is related to SiO_2 precipitation of free oxygen involved in dense and hot collisional cascades and produces the largest precipitates in the region where oxygen concentration is still high but primary events originating the collisional cascades are no longer sufficient to guarantee the spatial covering of the silicon. This mechanism prevails at relatively low fluence, while at high fluence the conventional precipitation dominates; in the present experimental conditions (energy $=100$ keV, target temperature $\simeq 250\,^{\circ}C$) the oxygen fluence separating these two behaviors is in the interval $1\times10^{16}-1\times10^{17}$ cm^{-2}.

I. INTRODUCTION

Despite the fact that silicon is one of the most studied substances and oxygen is its major contaminant, relatively little is known of the Si:O system, especially at high oxygen concentration ($>2\times10^{18}$ cm^{-3}) and temperature below 600 °C.

Single-crystal silicon is usually prepared by Czochralski (CZ) or float zone (FZ) techniques, with typical oxygen concentrations C of the order of 10^{18} cm^{-3} and 10^{16} cm^{-3}, respectively.[1] Oxygen in CZ silicon comes from SiO production at the Si(melt)-SiO_2 (crucible) interface and incorporation in the melt, and from preferential oxygen segregation in the crystal at the moving Si(crystal)-Si(liquid) interface.

Oxygen in silicon is known to be a covalently bonded interstitial; in this form (a two-dimensional rationalization is shown in Fig. 1) it is electrically inactive.

The diffusion of covalently bonded interstitial oxygen O_i in the temperature interval 350–1250 °C is an activated process with diffusion coefficient D given by

$$D(T)=D_0\exp(-E^*/k_BT)\ , \tag{1}$$

where T is the absolute temperature, k_B is the Boltzmann constant, $D_0=0.13$ cm^2/s, and $E^*=2.53$ eV.[2] Anomalously fast diffusing oxygen has hitherto been observed in two situations: in high fluence, ion-implanted silicon,[3–6] where it is believed to be in the form of molecular oxygen O_2 obtained after heat treatments at moderate temperature,[7] and in silicon exposed to atomic hydrogen, where oxygen diffusivity is presumably related to OH groups.[8]

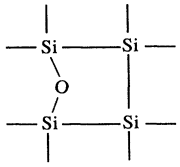

FIG. 1. Two-dimensional rationalization of covalently bonded interstitial oxygen in silicon.

The solubility C^{sol} of oxygen in silicon can be described by the formula

$$C^{sol}(T)=C_0^{sol}\exp(-\Delta E/k_BT)\ , \tag{2}$$

where $C_0^{sol}=9\times10^{22}$ cm^{-3} and $\Delta E=1.52$ eV. Equation (2) is accurate within a factor of 2 in the range 800–1400 °C; all experimental data can be collected in an Arrhenius plot within two straight lines with slope 1.26 and 1.80 eV.[2]

Since oxygen concentration in CZ silicon generally exceeds the solid solubility up to almost the melting point, oxygen can separate as SiO_2 provided that the duration of the thermal process is long enough to allow the formation of SiO_2 precipitates. Since SiO_2 has a molar volume approximately twice that of silicon, inner silicon oxidation takes place with the injection of self-interstitials Si_i,

$$(1+r)Si+2O_i\rightarrow SiO_2+rSi_i\quad (r\simeq1)\ , \tag{3}$$

provided that the crystal elastic energy associated with the stress generated by the SiO_2 precipitate exceeds the formation energy of the self-interstitial (Ref. 9, Ch. 3).

The electrical activity of oxygen is manifested by the formation of thermal donors, which are complexes involving four or more oxygen atoms formed after prolonged annealing at 500 °C with a rate faster than that permitted by standard oxygen diffusivity (though the formation-destruction kinetics are well characterized experimentally,[10] the microscopic structure of the thermal donor is, as discussed extensively by Bourret,[11] a problem not solved yet) and new thermal donors, which are oxygen complexes involving carbon formed after annealing at higher temperature;[10] oxygen is also suspected[12] to be responsible for the electron-hole pure generation phenomena discovered by Cerofolini and Polignano.[13,14]

There is a wide body of experimental knowledge of the structures formed after annealing of moderately supersaturated CZ silicon; as the annealing temperature T increases, the following complexes are known to be formed: vacancy-oxygen complexes (for $T=200-400\,^{\circ}C$), thermal

donors (around $T=500\,°C$), new thermal donors (for $T=600-900\,°C$), platelets (for $T=950-1050\,°C$), and eventually polyhedral SiO_2 precipitates (for $T \gtrsim 1100\,°C$).[15,16]

By far less known are the silicon-oxygen complexes formed in highly supersaturated silicon ($C > 10^{19}$ cm^{-3}). A way to explore which metastable structures are formed in this concentration domain is to insert the wanted amount of oxygen in the silicon crystal at low temperature and to study the evolution of the system after isothermal heat treatments. The most practical way to insert amounts of oxygen producing local concentrations in the range $10^{19}-10^{22}$ cm^{-3} in the crystal is ion implantation at fluences Φ in the range $10^{15}-10^{18}$ cm^{-2} at a temperature high enough to allow an appreciable reconstruction of the crystal, but not so high as to produce a large oxygen redistribution. A target temperature in the range 100–500 °C satisfies both these conditions.

II. EXPERIMENT

A. Sample preparation

Oxygen was implanted into single-crystal silicon by an Eaton NV-4206 medium-current ion implanter at an energy $E=100$ keV and fluence in the range $\Phi=1\times10^{15}-1\times10^{17}$ cm^{-2}. The target was formed by CZ-grown, n-type, 7–10-Ω cm resistivity, (100)-oriented, silicon slices of thickness 525 μm and diameter 10 cm. The silicon slices were tilted 7° or 15° with respect to the beam to minimize channeling effects. The typical current density was 100 μA/cm^2 with a rastered beam of area around 1 cm^2 covering the whole silicon area.

Unless otherwise stated, the data refer to samples obtained by implanting slices in poor thermal contact with the wafer holder. In this situation the temperature increased during the implantation, ranging from room temperature at $\Phi=0$ to around 150 °C at $\Phi\simeq1\times10^{15}$ cm^{-2}, eventually reaching approximately 250 °C for $\Phi\gtrsim2\times10^{15}$ cm^{-2}. This means that in all experiments with $\Phi>5\times10^{15}$ cm^{-2} most of the implantation was carried out in isothermal conditions at $T\simeq250\,°C$. In a few cases, care was taken to improve the thermal contact (by means of a conductive glue) and the wafer temperature was kept very close to 77 K by cooling the wafer holder with liquid nitrogen. Thermal cycles formed by isothermal steps were carried out in an inert atmosphere[17] in the temperature range 450–1200 °C, for a typical duration (8 h) much longer than the time required to ramp-up or ramp-down the furnace.

B. Analytical tools

The analyses of as-implanted and annealed samples were carried out by secondary-ion-mass spectrometry (SIMS) and transmission electron microscopy (TEM) in plan or cross-section views, in diffraction contrast or high-resolution (HREM) modes.

1. SIMS

The oxygen measurements were performed using a Cameca ims-4f ion microprobe equipped with cesium primary ion source. In order to avoid having to consider the artifacts produced by oxygen adsorption on the surface and by the knock-on effect, we limited our analysis to the depth region $x=50-400$ nm around the maximum of oxygen concentration.

2. TEM

The microscopic analysis was carried out in diffraction contrast, weak beam and HREM modes with a JEOL 2010 transmission electron microscope with a resolution limit of 0.23 nm, thus allowing the silicon crystal lattice to be imaged along the $\langle 110 \rangle$ direction. Observations were performed in plan view to give evidence for, and when possible to measure the density of, SiO_2 precipitates and lattice defects, and in the cross-section view to allow relevant thicknesses and depths to be determined.

III. EXPERIMENTAL RESULTS

In relation to the behavior of the implanted samples after annealing, it is convenient to describe separately the samples implanted in the "low-fluence" regime and in the "high-fluence" regime. It is anticipated that the behavior of SiO_2 precipitates in these two regimes is that sketched in Fig. 2. In this sketch two important depths are emphasized: x_{max}, the depth of maximum oxygen concentration, at which homogeneous precipitation takes place; and a depth $x_{\ddagger}(\Phi)$, at which "etherogeneous" precipitation takes place at fluence Φ. With etherogeneous precipitation we mean a kind of heterogeneous precipitation on preferential sites produced temporarily during the implantation itself (the *hot clouds* of Sec. IV). With the low-fluence regime we denote the fluence domain for which homogeneous SiO_2 precipitates are unstable and disappear after suitable annealing; with the high-fluence regime we denote the opposite situation.

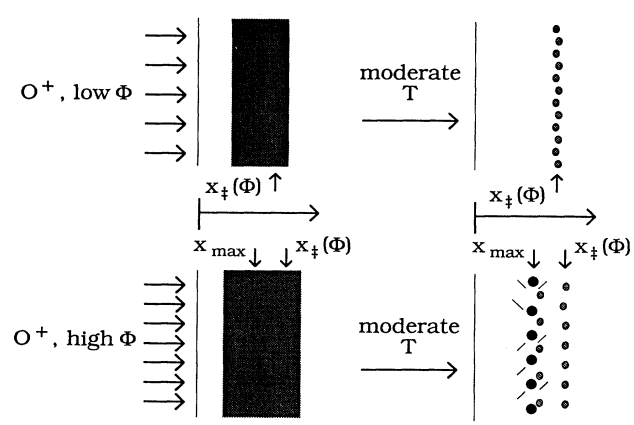

FIG. 2. Schematic behavior of SiO_2 precipitation in (a) low-fluence and (b) high-fluence samples.

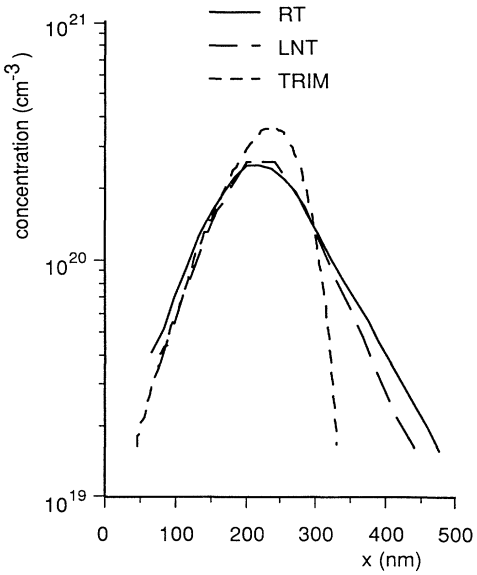

FIG. 3. Oxygen profiles in samples implanted at room temperature (RT) and liquid-nitrogen temperature (LNT) are compared with TRIM simulation. The LNT sample was stored at room temperature before SIMS analysis.

A. Low-fluence samples

The following considerations apply to samples implanted at floating temperature. For a comparison a sample was implanted at liquid-nitrogen temperature, with $E=100$ keV and $\Phi=5\times10^{15}$ cm^{-2}; this implantation produced a continuous amorphous layer centered on a depth of 205 nm with a thickness of 160 nm.

1. Oxygen profiles

Oxygen profiles of the samples implanted at $\Phi=5\times10^{15}$ cm^{-2} at floating temperature and at liquid-nitrogen temperature are presented in Fig. 3 together with the expected profile [obtained by transport of ions in matter (TRIM) simulation[18]] in an amorphous target. The oxygen profiles of samples implanted at lower fluence, 1×10^{15} cm^{-2} and 2×10^{15} cm^{-2}, were also determined and were found to scale linearly from that of the sample implanted at 5×10^{15} cm^{-2}.

2. SiO_2 precipitates

We shall refer to oxygen-related complexes, produced either during the implantation itself or after subsequent annealing, as SiO_2 precipitates without pretending that the fully stoichiometric compound is actually synthesized. Figure 4 shows the in-depth evolution after annealing of the damaged region in the sample implanted at $\Phi=5\times10^{15}$ cm^{-2}. From the comparison of the various photographs it is immediately realized that the damaged region is centered on the depth x_{max} of maximum oxygen concentration ($x\simeq220$ nm) with a thickness $\Delta x\simeq230$ nm in the as-implanted sample, and is shifted to a depth $x_{\ddagger}\simeq290$ nm after annealing at $T\geq650$ °C. The width of the damaged region is reduced with the annealing temperature, eventually reaching the value $\Delta x\simeq60$ nm after heating at 1200 °C.

The amount per unit area of SiO_2 precipitates was determined by plan-view analysis. For instance, Fig. 5 shows a plan view of the damaged region after annealing at 650 °C; the amount of SiO_2 precipitates contained in this sample is around 3×10^{11} cm^{-2}, the average diameter being (6 ± 1) nm, thus showing that practically all the contained oxygen is separated as SiO_2.

3. Silicon defects

Together with SiO_2 precipitates, other extended defects are also found, namely: {113} stacking faults (which are known to be produced during the implantation and to survive up to 750 °C), {100} defects, {111} stacking faults (observed after annealing at $T\geq750$ °C), and dislocations (produced after annealing at $T\geq750$ °C). The amounts of silicon atoms involved in {113}, {100}, and {111} extended defects are reported in Table I. This table is fully consistent with the interpretation for which {113} stack-

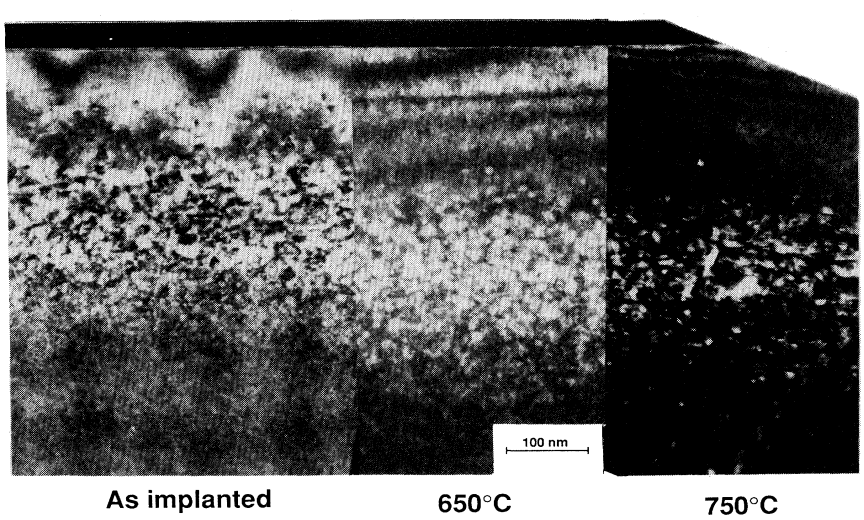

FIG. 4. Cross-section views of the implanted region in as-implanted and annealed samples; $\Phi=5\times10^{15}$ cm^{-2}, $E=100$ keV.

TABLE I. Defect amount per unit area $n_\square$ and average length L in specimens implanted at $\Phi = 5\times10^{15}$ cm^{-2}, $E = 100$ keV, in the as-implanted condition and after heat treatments. The asterisk indicates an estimated error of 50%. The dagger indicates uncertainty due mainly to the presence of a strong strain field and defect overlapping.

		As-implanted	650 °C	750 °C
{113} stacking faults				
	$n_\square$ (cm^{-2})	4×10^{12}	5×10^{12}	$\approx10^{12*}$
	L (nm)	5	10	8–10
{100} defects				
	$n_\square$ (cm^{-2})	$\approx10^{11\dagger}$	6×10^{11}	1×10^{12}
	L (nm)	5	10	10–80
{111} stacking faults				
	$n_\square$ (cm^{-2})			1.5×10^{10}
	L (nm)			10

ing faults evolve after annealing eventually forming {100} defects.[19]

B. High-fluence samples

The characterization of high-fluence samples is much less quantitative, essentially due to SiO_2 precipitates and silicon extended defects which are so numerous as to make impossible their density calculation (see, for instance, Fig. 6). However, the following conclusions can be drawn.

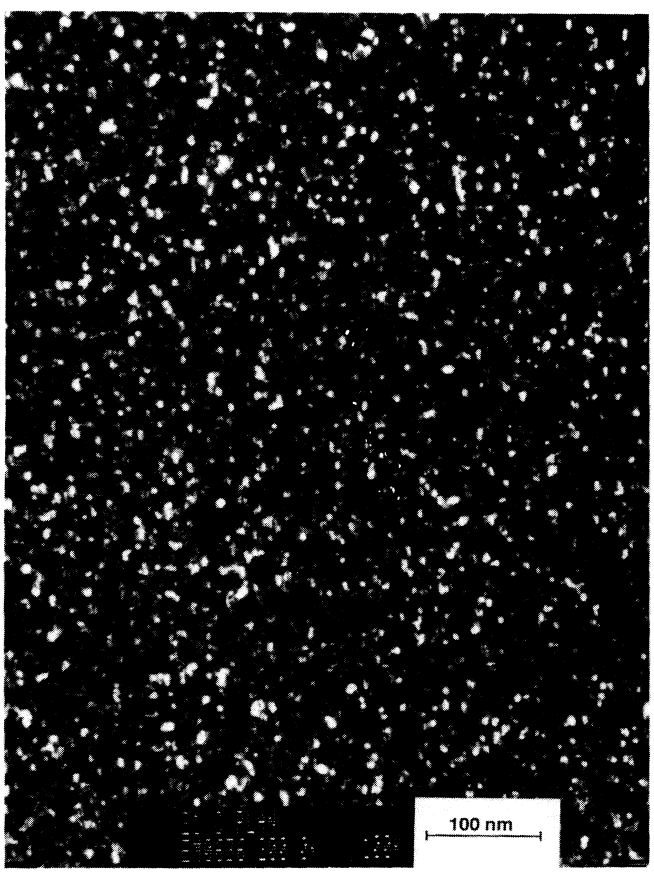

FIG. 5. Plan view of the implanted region in the sample implanted at $\Phi = 5\times10^{15}$ cm^{-2}, $E = 100$ keV and annealed at 650 °C.

1. *Oxygen profiles*

The oxygen profiles in as-implanted samples do not show large deviations from that observed at low fluence up to $\Phi = 1\times10^{17}$ cm^{-2}, thus showing that phenomena such as swelling, change of stopping power, sputtering, etc., though existing, are not very important yet.

2. *SiO_2 precipitates*

Two bands of SiO_2 precipitates are formed; after final annealing at 1000 °C they are sharply centered on the depths $x_{max} = 220$ nm and $x_{\ddagger} = 320$ nm, respectively (Fig. 7).

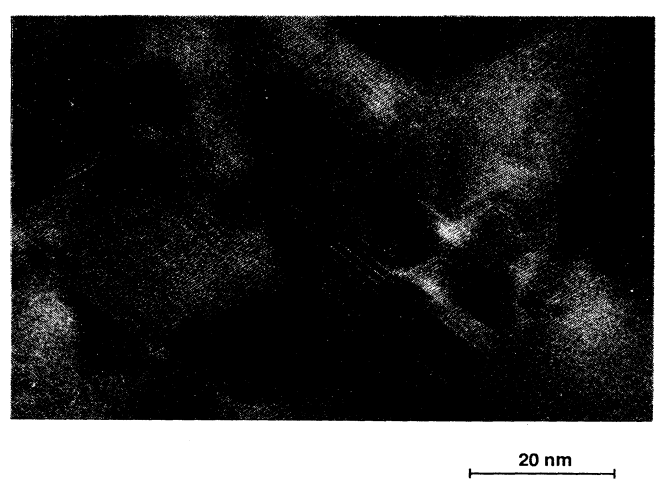

FIG. 6. High-resolution picture showing overlapping {111} stacking faults formed in the region of homogeneous precipitation after final annealing at 800 °C ($\Phi = 1\times10^{17}$ cm^{-2}, $E = 100$ keV).

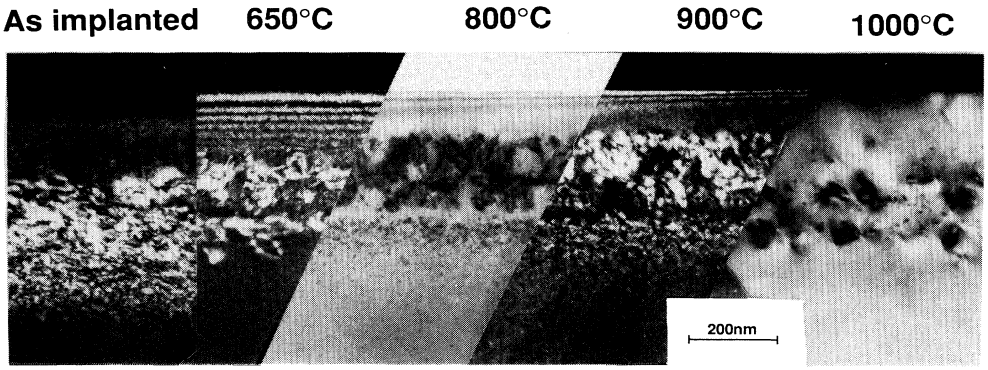

FIG. 7. Cross-section views of the implanted region in as-implanted and annealed samples; $\Phi = 1\times10^{17}$ cm^{-2}, $E = 100$ keV.

3. *Silicon defects*

In samples annealed first at 650 °C and henceforth at higher temperature in the range 800–1000 °C, the same defects and defect evolution observed in low-fluence samples are observed. However, the {111} defects are formed already at 650 °C; the amount of these defects is maximum after annealing at 800 °C (Fig. 6). The increase of amount and length of {111} stacking faults up to 800 °C suggests that SiO_2 precipitation is not completed up to this temperature. The decrease of the amount of {111} stacking faults at 900 °C suggests that the growth of precipitates takes place mainly through their coalescence rather than by further precipitation.

C. The border

Since even in low-fluence samples the oxygen concentration largely exceeds the solid solubility, precipitation is expected to occur even in this case. As discussed later, however, the nucleation mechanism produces very small precipitates which are dissolved after annealing unless they are so close as to coalesce and form larger precipitates. In our experimental conditions (energy, current density, and target temperature) the threshold fluence Φ_t dividing the behaviors sketched in Fig. 2 is in the interval 10^{16}–10^{17} cm^{-2}.

IV. FOUNDING THE MODEL

The development of the theory requires a brief summary of the concept of hot cloud, as stems from Refs. 20 and 21. We define *hot cloud* as the final, thermal stage of the collisional cascade. A collisional cascade, formed by binary collisions in an energy regime for which collisions take place with a mean free path of the order of the interatomic distance, becomes dense when it involves approximately $N_* \simeq 10^4$ atoms. From this stage on one can speak in terms of cascade temperature which decades asymptotically with time as $(t_0+t)^{-3/2}$ [because the cascade size increases in the quenching regime as $(t_0+t)^{1/2}$], t_0 being a characteristic time ($t_0 \approx 10^{-11}$ s) related to the minimum time required to render dense the cascade.[22] Most of the radiation damage is described in terms of maximum temperature T_* of the hot cloud. In turn, the maximum temperature is determined by the energy released in elastic collisions inside the smallest dense collisional cascade of diameter d_* (where $n_{Si}\pi d_*^3/6 = N_*$ and n_{Si} is the silicon atomic density, $n_{Si} = 5\times10^{22}$ cm^{-3}). This picture is applied to the formation of SiO_2 by assuming that precipitation is possible when the hot-cloud temperature T_* exceeds a critical temperature $T_\ddagger$.

The problem of calculating the maximum hot-cloud temperature is attacked as follows. Assume, temporarily, that the energy ϵ of the projectile originating the cascade is so high that on an average the projectile stops outside the minimum hot cloud, i.e., its range $R(\epsilon)$ is appreciably higher than the cascade diameter d_*. Therefore, only a few projectiles have a fate allowing them to impart all the energy they lose in elastic collisions to the hot cloud; only when the projectile stops in the minimum volume V_* of the hot cloud itself [$V_* = \frac{4}{3}\pi(d_*/2)^3$] does all the projectile energy imparted to the crystal in elastic collisions (the electronic energy loss not being responsible for heating the collisional cascade[20,21]) contribute to heating the collisional cascade itself. This means that only a fraction of projectiles with kinetic energy greater than ϵ are useful to form dense collisional cascades with the required temperature.

Let $\eta_{Si}(\epsilon)$ be this fraction for silicon recoils and $\eta_O(\epsilon)$ the fraction of oxygen projectiles stopping in the volume V_*; these quantities can be estimated by direct TRIM simulations at different energies (Fig. 8). The "effective hot-cloud yield" $y(x,\epsilon)$ (i.e., the yield of collisional cascades where all the energy lost in elastic collisions is imparted to the hot cloud of minimum size) is then given by[23]

$$y(x,\epsilon) = \eta_O(\epsilon)\chi(x,\epsilon) + \eta_{Si}(\epsilon)Y(x,\epsilon) ,$$

where $\chi(x,\epsilon)$ is the projectile concentration per unit fluence at depth x with energy ϵ and $Y(x,\epsilon)$ is the total recoil concentration per unit fluence. Figure 9 shows graphs $y(x,\epsilon)$ versus depth x, with the energy ϵ as parameter.

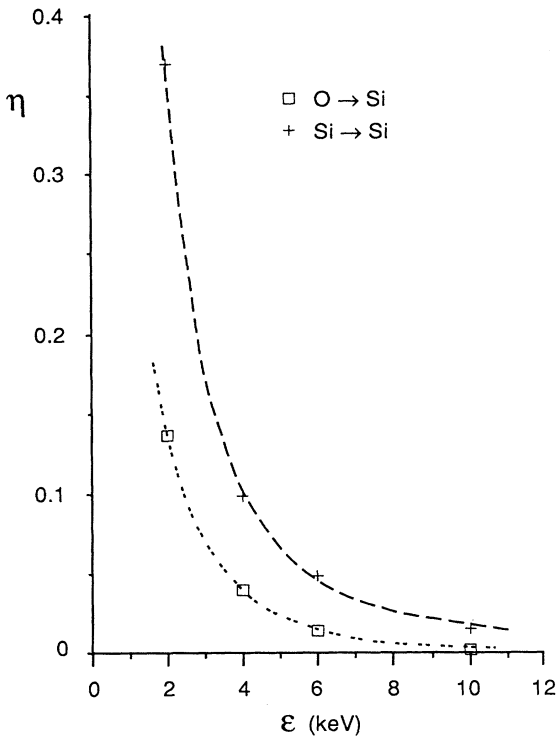

FIG. 8. Probability that silicon or oxygen stop inside the minimum-size hot cloud they produce as a function of projectile energy.

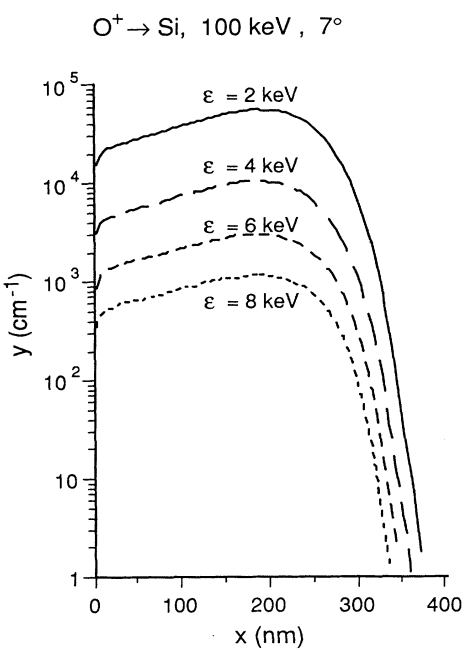

FIG. 9. Effective hot-cloud yield as a function of depth with energy as a parameter.

The function $y(x,\epsilon)$ allows us to define the yield of formation of SiO_2 precipitates,

$$y_{\ddagger}(x)=\eta_{O}(\epsilon_{\ddagger})\chi(x,\epsilon_{\ddagger})+\eta_{Si}(\epsilon_{\ddagger})Y(x,\epsilon_{\ddagger}) ,$$

where $\epsilon_{\ddagger}$ is the minimum energy producing a hot cloud with maximum local temperature $T_{\ddagger}$ high enough to allow for SiO_2 precipitation. The concentration per unit fluence of projectiles at rest, $\chi(x,\epsilon=0)$, will henceforth be denoted by the symbol $\chi_0(x)$.

A. Formation kinetics of SiO_2 precipitates

Once the yield $y_{\ddagger}(x)$ is known, the amount of SiO_2 complexes as a function of the fluence is determined as follows. The change of oxygen concentration $dC_p(x)$ due to oxygen separation as SiO_2 produced by effective hot clouds in the elementary implantation step of fluence $d\Phi$ is given by

$$dC_p(x)=V_*[C(x)-C_p(x)]y_{\ddagger}(x)d\Phi , \tag{4}$$

where $C(x)-C_p(x)=\chi_0(x)\Phi-C_p(x)$ is the concentration of available oxygen involved in effective hot clouds.

Defining $\Phi_{\ddagger}(x)=1/V_*y_{\ddagger}(x)$ and setting the initial condition $C_p=0$ when $\Phi=0$, the solution of Eq. (4) is

$$C_p(x)=\chi_0(x)\Phi_{\ddagger}(x) \times\left\{\frac{\Phi}{\Phi_{\ddagger}(x)}-\left[1-\exp\left[-\frac{\Phi}{\Phi_{\ddagger}(x)}\right]\right]\right\} , \tag{5}$$

which exhibits the following asymptotic behaviors:

$$C_p(x)\simeq\chi_0(x)\Phi^2/2\Phi_{\ddagger}(x) \quad \text{for } \Phi\lesssim\Phi_{\ddagger}(x)$$

and

$$C_p(x)\simeq\chi_0(x)[\Phi-\Phi_{\ddagger}(x)] \quad \text{for } \Phi\gg\Phi_{\ddagger}(x) .$$

B. Nucleation mechanism

By the addition of a convenient hypothesis, explaining the fate of precipitates involved in new hot clouds, the model can be extended to predict the average density $n_p(x)$ and size $d_p(x)$ of the produced SiO_2 precipitates. The hypothesis we assume is that an *effective hot cloud investing an already formed precipitate does not destroy it, but rather produces another precipitate with the available oxygen.* This hypothesis can be restated by saying that *inside a hot cloud, homogeneous precipitation prevails on heterogeneous precipitation on preexisting precipitates* (a possible explanation of this quite-extravagant assumption will be given in the last statement of the Appendix). In this hypothesis the density of precipitates is given by

$$n_p(x)=y_{\ddagger}(x)\Phi , \tag{6}$$

so that, for any given energy $\epsilon_{\ddagger}$, the density distribution of precipitates copies the profile $y_{\ddagger}(x)$. In the region where effective hot clouds produce SiO_2 precipitates, their diameter is given by

$$d_p(x)=2\left[\frac{3}{4\pi}\frac{N_O(x)}{n_O}\right]^{1/3}, \tag{7}$$

where $N_O(x)$ is the number of oxygen atoms in the precipitate and n_O is close to the atomic density of oxygen in SiO_2 ($n_O=4.4\times10^{22}$ cm^{-3}). In turn, $N_O(x)$ can be calculated as a piecewise function of x, by distinguishing regions where effective hot clouds are, on the mean, spatially superimposed, from regions where hot clouds do not cover completely the space. The probability of spatial superimposition of hot clouds can be either of the order of unity or negligible in relation to the fact that the amount of effective hot clouds generated per unit volume, $y_\ddagger(x)\Phi$, exceeds or does not exceed the critical value $n_*=n_{Si}/N_*$, which guarantees the full covering of the region of interest. The critical depth $x_\ddagger$, where spatial superimposition is no longer complete, is given by the condition

$$y_\ddagger(x)\Phi=n_* , \tag{8}$$

which, considered as an equation for x, may have (see Fig. 9) no solution (for $\Phi<n_*/y_{\ddagger\max}$), one solution [for $\Phi>n_*/y_\ddagger(0)$], or two solutions [for $n_*/y_{\ddagger\max}\le\Phi\le n_*/y_\ddagger(0)$]. In the second case we denote the solution of Eq. (8) as $x_\ddagger=x_\ddagger(\Phi)$. The number of oxygen atoms in each precipitate is therefore given by

$$N_O(x)=\begin{cases}\chi_0(x)/y_\ddagger(x) & \text{for } x<x_\ddagger(\Phi)\\ \chi_0(x)\Phi N_*/n_{Si} & \text{for } x\ge x_\ddagger(\Phi)\ .\end{cases} \tag{9}$$

Due to the relatively flat behavior of $\chi_0(x)$ at $x=x_\ddagger(\Phi)$, $N_O(x)$ and $d_p(x)$ have maxima centered on $x_\ddagger(\Phi)$.

V. VALIDATING THE MODEL

The predictions of the model about depth location of precipitates and threshold fluence for precipitate coalescence are considered in this section.

A. Density and size of SiO_2 precipitates

The model hitherto developed speaks about nucleation phenomena during the implantation. It is, however, expected that an annealing process after the implantation will result in growth of large precipitates and dissolution of small precipitates. Since the largest precipitates are located at $x_\ddagger(\Phi)$ rather than at x_{max}, our model can be tested versus the current mode of nucleation by annealing an as-implanted sample.

Figure 10 shows a TEM cross section of a sample implanted at $\Phi=5\times10^{15}$ cm^{-2} and annealed at $T=1200\,°C$. The inspection of this photograph shows that the SiO_2 precipitates are located at $x=(290\pm30)$ nm; this depth is reproduced by assuming an energy $\epsilon_\ddagger=5^{+1.5}_{-2.5}$ keV. In turn, the knowledge of $\epsilon_\ddagger$ allows us to calculate from Eq. (6) the average density $n_p(x)$ and from Eqs. (7) and (9) the diameter $d_p(x)$ of the so-produced SiO_2 precipitates (Figs. 11 and 12, respectively).

Figure 13 shows a TEM cross section of a sample implanted at $\Phi=1\times10^{17}$ cm^{-2} and annealed at 1000 °C; the picture shows that the energy $\epsilon_\ddagger$ which allows for the precipitation region at 290 nm in the sample implanted at 5×10^{15} cm^{-2} gives $x_\ddagger(\Phi)=320$ nm at 1×10^{17} cm^{-2}, thus accounting for the precipitation region centered on depth of (325 ± 25) nm.

The energy $\epsilon_\ddagger$ so determined is of the same order as the amphorization energy in silicon,[20,21] i.e., $\epsilon_\ddagger$ is an energy able to displace permanently silicon atoms from their lattice positions. Since the energy required to break Si-O bonds is much larger, it is expected that these hot clouds are unable to destroy preexisting precipitates, therefore

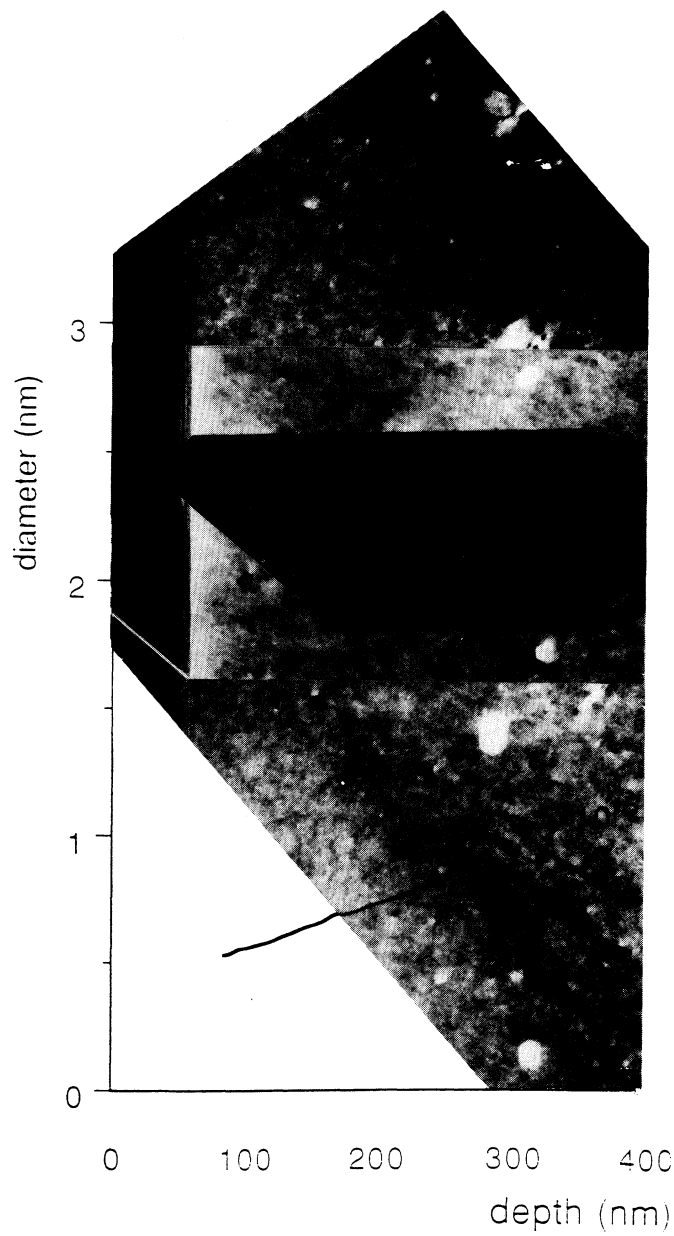

FIG. 10. Cross-section view of precipitates remaining after annealing at 1200 °C of the sample implanted at 5×10^{15} cm^{-2}, superimposed on the calculated diameter profile of precipitates produced in as-implanted conditions.

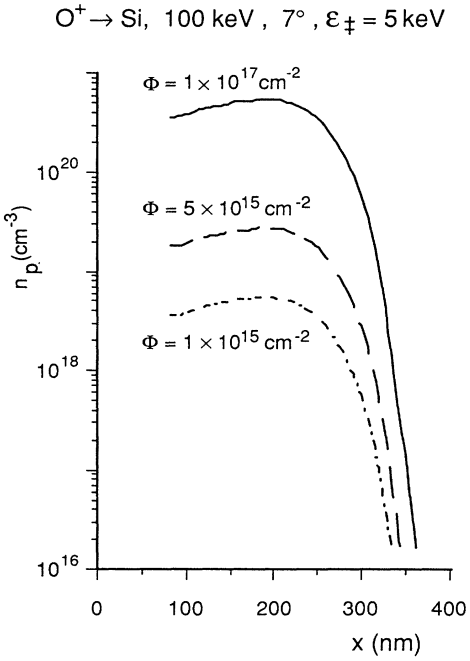

FIG. 11. Concentration of precipitates vs depth taking fluence as parameter.

upholding *a posteriori* the hypothesis that SiO_2 precipitates are not destroyed when invested by a hot cloud.

B. The threshold fluence

Figure 7 also shows the existence of a second precipitation region centered on x_{max} not present in the sample

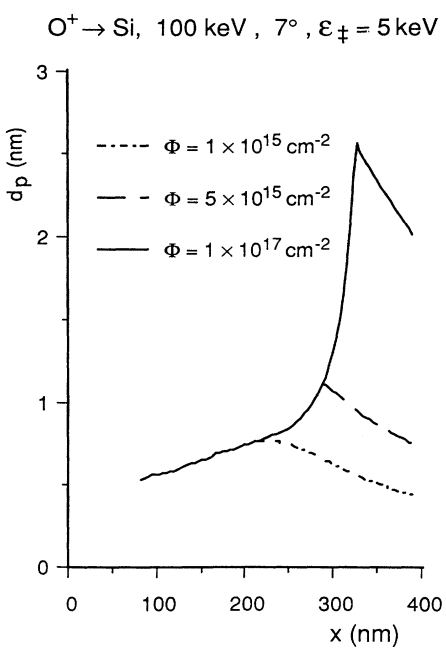

FIG. 12. Diameter of precipitates vs depth taking fluence as parameter.

implanted at $\Phi = 5\times10^{15}$ cm^{-2}. The problem of predicting the lowest value of fluence at which homogeneous precipitation prevails on etherogeneous precipitation is not of easy solution and can be attacked on statistical grounds.[24]

Consider, for any Φ, the diameter $d_p[x_\ddagger(\Phi)]$ of precipitates formed at $x = x_\ddagger(\Phi)$ and define for a sake of compactness $d_0(\Phi) = d_p[x_\ddagger(\Phi)]$; while the diameter of these precipitates increases with Φ, their concentration n_* is a constant. Precipitates formed at x_{max} are much smaller and closer to one another; two of them may be considered to form a *connected cluster* when they are separated by a distance smaller than d_{Si} (where d_{Si} is the silicon diameter, $d_{Si} = 0.234$ nm); they will be considered to form an *adjacent set* when they are separated by a distance between d_{Si} and $2d_{Si}$.

Consider now a covering of the region around x_{max}, obtained by sampling cubes each of edge $d_0(\Phi)$, and the volume occupied by a set of k adjacent precipitates. It is not unrealistic to assume that homogeneous precipitation

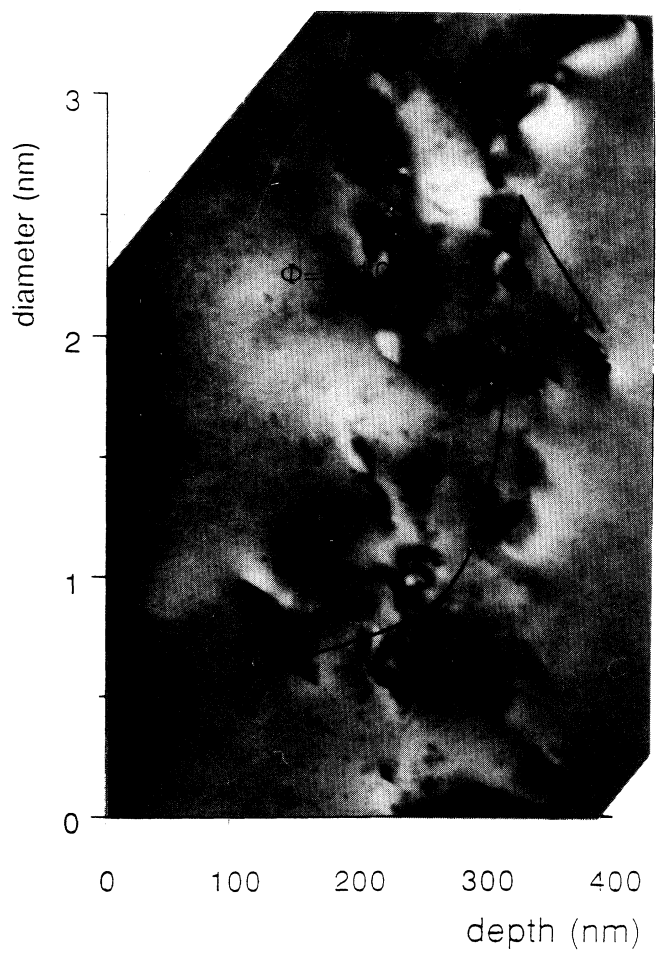

FIG. 13. Cross-section view of precipitates remaining after annealing at 1000 °C of the sample implanted at 1×10^{17} cm^{-2}, superimposed on the calculated diameter profile of precipitates produced in as-implanted conditions.

prevails when the density n_k of sampling cubes containing sets with k adjacent precipitates with total volume higher than $\pi d_0(\Phi)^3/6$ exceeds n_*. Indeed, in the early stages of annealing small precipitates are dissolved and the oxygen they release is captured either by precipitates at $x_\ddagger$ [with a total cross section around $\pi(d_0/2)^2 n_* \Delta_*$, where Δ_* is the thickness of the region where precipitates are dispersed] or by adjacent sets with k precipitates at $x_{\max}$ [with a total cross section around $\pi(d_k/2)^2 n_k \Delta_{\max}$, where $\Delta_{\max}$ is the thickness of the region where precipitates are dispersed], since the capture of oxygen atoms by adjacent sets transforms them in connected clusters with the same size. The condition for thermodynamic stability of these precipitates is therefore that their diameter d_k exceeds d_0 and the condition for their prevalence is that their collection efficiency is higher than that at $x_\ddagger$, i.e., $\pi(d_k/2)^2 n_k \Delta_{\max} > \pi(d_0 2)^2 n_* \Delta_*$. Combining these conditions one has $n_k \gtrsim n_*$, provided that $\Delta_{\max} \simeq \Delta_*$.

The minimum value $\bar{k}$ of k satisfying the above conditions is that for which homogeneous precipitation prevails on the etherogeneous one. The value of $\bar{k}$ must satisfy the conditions

$$\left[\frac{d_0}{d_p(x_{\max})+2d_{\mathrm{Si}}}\right]^3 \le \bar{k} < \left[\frac{d_0}{d_p(x_{\max})+d_{\mathrm{Si}}}\right]^3 ,$$

while the concentration n_k can be calculated by assuming that precipitates are distributed spatially according to the Poisson statistics. In this case, n_k is obtained dividing the probability of having k precipitates in the volume,

$$P_k = (m^k/k!)\exp(-m)$$

[where m is the average number of precipitates in the sampling cubes, $m = y_\ddagger(x_{\max})\Phi d_0(\Phi)^3$] by the sampling volume d_0^3.[24] The condition $P_k(\Phi)/d_0(\Phi)^3 \ge n_*$ is an equation in Φ, whose solution, $\Phi_t = (1.6\text{–}2.5)\times 10^{16}$ cm^{-2}, is in agreement with the experimental data (see Sec. III C).

VI. DISCUSSION

While at relatively low temperature (say, below 600 °C) oxygen forms mainly complexes with vacancies,[15] at temperatures high enough to allow for appreciable oxygen diffusion, precipitation becomes possible and SiO_2 becomes the prevailing structure.[16] Since the oxidation number of oxygen does not vary during precipitate growth, the precipitation of SiO_2 in silicon can be regarded as diffusion limited. The standard description of diffusion-limited growth of precipitates, essentially due to Ham,[25] requires the knowledge of the initial radius and density of precipitates. In turn, information on these quantities is usually obtained from the Volmer and Weber theory of nucleation.[26]

In this theory, the free-energy difference $\Delta F(d_p)$ of a precipitate of diameter d_p with respect to the solution has two contributions: one negative and increasing as d_p^3, and the other positive and increasing as d_p^2. Since $\Delta F(d_p) \propto d_p^2$ for small d_p and $\Delta F(d_p) \propto d_p^3$ for large d_p, surface effects will prevail for small precipitates while volume effects will prevail for big precipitates. There is therefore a critical diameter d_{pc} separating these regions. The theory of nucleation specifies the number of precipitates with diameter d_{pc} as

$$n_{\mathrm{pc}} = n_s \exp[-\Delta F(d_{\mathrm{pc}})/k_B T] , \tag{10}$$

where n_s is a concentration related to the density of nucleation sites.

The usual way to produce a theory of precipitate growth is to assume that at time $t=0$ the density of precipitates is given by the density of nuclei with critical radius. The combination of Ham's theory of precipitate growth and the Volmer and Weber theory of nucleation can be inserted in standard simulation codes for impurity diffusion. A version of SUPREM III,[27] modified to describe in the above framework precipitation phenomena in supersaturated silicon, was demonstrated to give an accurate description of boron concentration in supersaturated Si:B.[28] Its application to the highly supersaturated Si:O system, however, does not describe precipitation at $x_\ddagger$.

In the model developed here, this precipitation is ascribed to an initial condition different from that predicted by the Volmer and Weber theory of nucleation. While in the Volmer and Weber theory the formation of nuclei is, according to Eq. (10), driven by the heat reservoir temperature, in our model the initial condition results from the interaction of an intrinsically thermal phenomenon (the hot cloud), substantially uncoupled with the heat reservoir.

Since the thermal stage of the collisional cascade is intrinsic to the stopping mechanism of implanted ions, it may reasonably be concluded that *in all samples implanted at a fluence high enough to produce a supersaturated solution, nuclei are formed with a distribution differing appreciably from that predicted by the standard theory of nucleation.* This conclusion is especially important because in most situations supersaturation is obtained by high-fluence implantation. Of course, since the effective temperatures required to form the precipitate may be different for different impurities, the hot-cloud distribution and temperatures may vary from one projectile to another, and consequently the as-implanted distribution of precipitates is expected to differ from one situation to another.

The second observation concerns the method used for determining under which conditions homogeneous precipitation prevails on etherogeneous precipitation. Though the proposed model seems to work only for ion implantation, it can also be extended to understand under which conditions homogeneous precipitation prevails on heterogeneous precipitation in a supersaturated solution. Indeed, in this case a comparison is established between preexisting heterogeneous precipitates (whose average diameter d_0 and density n_0 are supposed to be known) and the distribution of homogeneous precipitates with critical diameter d_{pc} and density n_{pc}, both depending on temperature and concentration. The condition of prevalence of homogeneous precipitation is therefore obtained by sampling the space with cubes with edge d_0 and searching the temperature T allowing for a distribution whose density of adjacent sets with diameter greater than d_0 exceeds n_0.

VII. CONCLUSIONS

An experimental and theoretical study of the Si:O system obtained by high-fluence oxygen implantation has been carried out. This study has given evidence for SiO_2 precipitation produced during oxygen implantation by dense and hot collisional cascades.

A theoretical, quantitative description has been proposed, in the light of a model of nucleation produced in the thermal stage of collisional cascades. This model predicts the dependence on depth of density and size of precipitates separated during implantation; the maximum of precipitate size is centered on a depth where oxygen concentration is still high but primary events originating the collisional cascades are no longer sufficient to guarantee the spatial covering of the silicon. Theoretical predictions agree with experimental TEM data.

ACKNOWLEDGMENTS

We are indebted to Dr. S. Solmi (Instituto LAMEL-CNR, Bologna) for modified SUPREM III simulation of oxygen diffusion and precipitation; SIMS analyses were carried out by Dr. R. Canteri (IRST, Povo TN).

APPENDIX: EXPECTED REACTIONS OF OXYGEN WITH POINT DEFECTS

Oxygen is expected to react easily with both vacancies and self-interstitials. Though there is no general consensus on structural, thermodynamic, and kinetic properties of both these defects (Ref. 9, Ch. 2), the following considerations are sufficiently robust to be independent of the exact value of formation energy and entropy and activation energy and entropy for migration. It is an additional fundamental stipulation, however, that two kinds of self-interstitials exist: the purely T_d self-interstitial, which is assumed to be formed at relatively low temperature (say, below 700 K), and the dumbbell self-interstitial, which is assumed to be formed at higher temperature.

For most of the forthcoming qualitative considerations we make the following assumptions:

(i) Enthalpy differences are calculated from bond energies.

(ii) The following values of bond energies are assumed: $E(\text{Si—Si})=2.4$ eV (reported values range in the interval 2.2–2.6 eV), $E(\text{Si—O})=3.8$ eV, and $E(\text{O=O})=5.2$ eV.[29]

(iii) All corrections to these bond energies due to lattice relaxation, bond distortion, etc. are ignored unless the enthalpy difference between two configurations is more than 1 eV (which is the estimated uncertainty of our considerations).

(iv) When the electronic energies of two different configurations are approximately the same (i.e., when their difference is less than 1 eV), the most stable configuration will be decided on manifestly evident criteria of minimum stress.

These assumptions are sufficient to have information on the stability and reactivity of most of the considered configurations.

1. Vacancy-oxygen reactions

The vacancy (v) is a preferred site to trap oxygen by formation of oxygen bridges on the deformed Si-Si bonds of the vacancy (Fig. 14). For *covalently bonded oxygen* the stability of both the simply decorated vacancy, v-O [evidence for which was given by Watkins and Corbett in 1961 (Ref. 30)], and the doubly decorated one, v-O_2 [which is formed after annealing at temperature higher than 300 °C (Ref. 31)], are guaranteed by the relief of stress associated with the undecorated vacancy. That the oxidated vacancy has a lower stress than both the undecorated vacancy and the two O_i is immediately realized by comparing the Si-Si distance between next-nearest neighbors, 0.383 nm, with the Si-O-Si length for a linear arrangement, 0.366 nm, the covalent Si-Si distance being 0.234 nm. The doubly decorated vacancy is more stable than the singly decorated vacancy; the very fact that the distance between oxygen-bridged silicon atoms is almost exactly forced to the lattice distance stresses the other Si-Si bond in the vacancy; this is the presumable reason why the v-O complex is paramagnetically active.[30]

The fully oxidated vacancy v-O_2 is unstable in the presence of T_d silicon interstitials, because though the reaction (Fig. 15)

$$v\text{-}O_2+\text{Si}(T_d)\rightarrow O_2$$

has an approximately null enthalpy difference, $\Delta H \simeq 4E(\text{Si—O})-4E(\text{Si—Si})-E(\text{O=O})=0.4$ eV, the stress associated with interstitial O_2 (maximum size $\simeq 0.24$ nm) is, however, expected to be much smaller than that associated with T_d silicon (diameter $=0.234$ nm) and v-O_2.

2. Self-interstitial–oxygen reactions

Several self-interstitial configurations seem possible; among them we quote the pure T_d self-interstitial, which is expected to be a fast diffuser,[32] and the dumbbell self-interstitial[33]

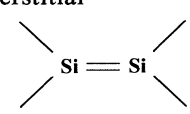

which might be the species relatively immobile up to 10^3

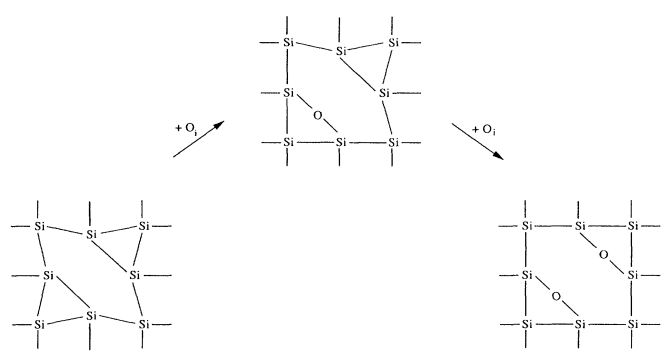

FIG. 14. The formation of oxygen-vacancy complexes by consecutive reactions with oxygen. The progressive loss of lattice distortion is emphasized.

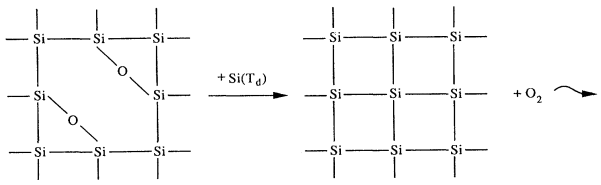

FIG. 15. Formation of molecular oxygen by reaction of a doubly decorated vacancy with a T_c self-interstitial.

K.[34] Information on the relative stabilities of T_d and dumbbell self-interstitials cannot be obtained with the above elementary considerations because the electronic configuration of each dumbbell silicon is given by three sp^2 hybrid orbitals lying in the same plane and one p orbital perpendicular to it, while the T_d self-interstitial has presumably a $3s^2 3p^2$ outer electronic configuration.

Though silicon has a very poor tendency to form π double bonds,[29] the existence of the dumbbell self-interstitial is strongly supported by the recent discovery of disilenic compounds and their chemistry.[35] Though disilene itself $H_2Si{=}SiH_2$ is unstable, provided that the Si=Si double bond is protected by the replacement of hydrogen with a suitably large radical R, compounds $R_2Si{=}SiR_2$ stable up to 170 °C can be isolated. The availability of these compounds has allowed the silicon double bond to be studied.

The Si=Si double bond has a length of 0.214–0.216 nm and an energy of 2.3–2.5 eV. Comparing these values with the length and energy of the simple bond, 0.234 nm and 2.2–2.6 eV, respectively, the relative stability of the double bond is confirmed. In spite of its relative stability, the Si-Si π bond is rather reactive, the activation energy required to open it being a fraction of an eV.

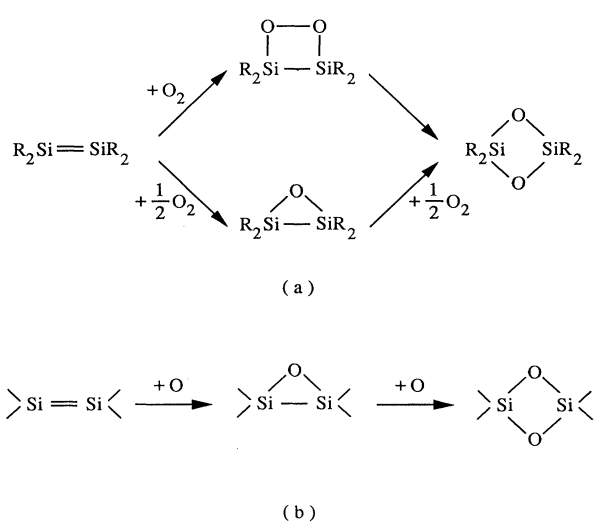

FIG. 16. The formation of cyclodisiloxanes (a) by oxidation of disilenes, and (b) by oxidation of a dumbbell self-interstitial.

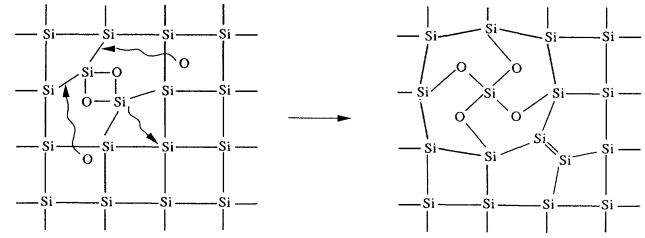

FIG. 17. Formation of a coherent precipitate by oxidation of a cyclodisiloxane ring and injection of a dumbbell self-interstitial.

Disilenic compounds are known to react with oxygen according to the scheme of Fig. 16(a) to eventually form cyclodisiloxanes, so that it is highly plausible that the dumbbell self-interstitial reacts readily with molecular or covalently bonded interstitial oxygen to form cyclodisiloxane, as shown in Fig. 16(b).

A model for SiO_2 precipitation

The dumbbell self-interstitial is a preferential site for oxygen precipitation if one stipulates that the highly strained heterocycle of Fig. 16(b) (with angle Si-O-Si = 86°–98° and Si-Si distance of 0.231–0.245 nm) reacts further with atomic or molecular oxygen to form a SiO_4 complex (where silicon coordination is the same as in silica) with the injection of a self-interstitial (Fig. 17). This injection restores the initial condition on the contour of the SiO_4 complex so that the process can continue up to the formation of a SiO_2 precipitate.

It is interesting to remark that this mechanism does not inject net self-interstitials until the SiO_4 complex remains coherent with the matrix; this mechanism will terminate when the energy excess accumulated in this complex exceeds the formation energy of a self-interstitial. At this point reaction (3) will be activated and the precipitate will lose its coherence with the crystal.

According to this mechanism, SiO_2 precipitation is characterized by three phases.

(i) *An induction phase,* where the number of self-interstitials remains constant so that the reaction proceeds smoothly via the mechanism sketched in Fig. 17.

(ii) *An early autocatalytic growth phase,* in which the number of self-interstitials, which are the seeds for oxygen separation as SiO_2, increases as the reaction proceeds but remains so small that they can remain localized at the growing Si-SiO_2 interface.

(iii) *A final autocatalytic growth phase,* in which the number of self-interstitials (which increases with precipitate volume, i.e., with the third power R^3 of precipitate radius R) exceeds the number of available sites at the Si-SiO_2 interface (which increases with R^2).

The precipitate radius $\bar{R}$ separating the early autocatalytic phase from the final autocatalytic phase is given by

$\bar{R} \simeq 3\lambda/r$, where r is the number of self-interstitials injected per newly formed SiO_2 molecule and λ is the thickness of the interface layer in which the self-interstitials are arranged.

Two situations can be hypothesized. At temperature so low as to forbid self-interstitial diffusion, precipitation can continue (R increases) only if the width λ of the interface region increases correspondingly; this low-temperature precipitation leads to precipitates surrounded by an interstitial-rich atmosphere. At higher temperature, self-interstitials will, however, diffuse and organize in defects of extrinsic type (e.g., {111} stacking faults) which react further with oxygen to form a platelike silicon-oxygen complex.

This overall process is expected to proceed only at temperatures sufficiently high to allow the dumbbell configuration of the self-interstitial. Interestingly enough, internal gettering processes (in which the precipitates are formed by prolonged annealing at moderate temperature) are usually carried out in the temperature range 700–800 °C (Ref. 9, Ch. 9).

At last, we observe that the idea that dumbbell self-interstitials are preferential sites for the formation of SiO_2 precipitates is consistent with the assumption that precipitation in a hot cloud does not take place heterogeneously on a preexisting precipitate, but rather on preexisting clusters of dumbbell self-interstitials, possibly formed when a few native T_d self-interstitials are invested by a hot cloud and hence brought to the configuration stable at high temperature. Though this SiO_2 precipitation takes place heterogeneously on preexisting sites, it mimics homogeneous precipitation because small clusters of self-interstitials are not directly accessible to electron microscopy.

---

*On leave from the Department of Physics, University of Milano, Milano, Italy.

[1]W. Zuhlener and D. Huber, Crystals **8**, 1 (1982).

[2]J. C. Mikkelsen, in *Oxygen, Carbon, Hydrogen and Nitrogen in Crystalline Silicon,* edited by S. J. Pearton, J. W. Corbett, J. C. Mikkelsen, and S. J. Pennycook, MRS Symposia Proceedings No. 59 (Materials Research Society, Pittsburgh, 1986), p. 19.

[3]S.-T. Lee and D. Nichols, Appl. Phys. Lett. **47**, 1001 (1985).

[4]S.-T. Lee and P. Fellinger, Appl. Phys. Lett. **49**, 1793 (1986).

[5]S.-T. Lee, P. Fellinger, and S. Chen, J. Appl. Phys. **63**, 1924 (1988).

[6]L. Meda, S. Bertoni, G. F. Cerofolini, C. Spaggiari, and R. Canteri, in *Silicon-On-Insulator Technology and Devices,* edited by W. E. Bailey (The Electrochemical Society, Pennington, NJ, 1992), p. 237.

[7]U. Gösele, K. Y. Ahn, B. P. R. Marion, T. Y. Tan, and S.-T. Lee, Appl. Phys. A **48**, 219 (1989).

[8]R. C. Newman, A. R. Brown, R. Murray, A. Tipping, and J. H. Tucker, in *Semiconductor Silicon 1990,* edited by H. R. Huff, K. G. Barraclough, and J. Chikawa (The Electrochemical Society, Pennington, NJ, 1990), p. 734.

[9]G. F. Cerofolini and L. Meda, *Physical Chemistry Of, In and On Silicon* (Springer-Verlag, Berlin, 1989).

[10]V. Cazcarra and P. Zunino, J. Appl. Phys. **51**, 4206 (1980).

[11]A. Bourret, in *Proceedings of the 13th International Conference on Defects in Semiconductors,* edited by L. C. Kimerling and J. M. Parsey (The Metallurgical Society, Warrendale, PA, 1985), p. 129.

[12]P. Pellegrini, J. Appl. Phys. **71**, 5504 (1992).

[13]G. F. Cerofolini and M. L. Polignano, J. Appl. Phys. **55**, 3823 (1984).

[14]G. F. Cerofolini and M. L. Polignano, Appl. Phys. A **50**, 273 (1990).

[15]T. Gregorkiewicz and H. H. P. Th. Bekman, Mater. Sci. Eng. B **4**, 291 (1989).

[16]F. A. Ponce and S. Hahn, Mater. Sci. Eng. B **4**, 11 (1989).

[17]The atmosphere was slightly contaminated by an air leakage; this leakage did not produce appreciable silicon oxidation except at 1200 °C. All presented depth data are corrected by the grown surface oxide.

[18]J. F. Ziegler, TRIM 1989, version 5.3.

[19]A. Bourret, in *Microscopy of Semiconducting Materials,* edited by A. G. Cullis and P. D. Augustus, IOP Conf. Proc. No. 87 (Institute of Physics and Physical Society, London, 1987), p. 39.

[20]G. F. Cerofolini and L. Meda, Phys. Rev. B **36**, 5131 (1987).

[21]G. F. Cerofolini, L. Meda, and C. Volpones, J. Appl. Phys. **63**, 4911 (1988).

[22]H. Hsieh, T. Diaz de la Rubia, R. S. Averback, and R. Benedek, Phys. Rev. B **40**, 9986 (1989).

[23]The theory of amorphization by hot clouds as formulated in Refs. 20 and 21 is actually an oversimplification because it assumes at $\epsilon = 5$ keV the following efficiencies: $\eta_{Si} = 1$ and $\eta_x = 0$ or 1 according to projectile weight ($\eta_x = 0$ for projectile lighter than silicon and $\eta_x = 1$ otherwise). How approximate this description is can be understood by inspecting Fig. 8.

[24]W. Feller, *An Introduction to Probability Theory and Its Applications,* 3rd ed. (Wiley, New York, 1968).

[25]F. S. Ham, J. Appl. Phys. **30**, 1518 (1959).

[26]M. Volmer and A. Weber, Z. Phys. Chem. **119**, 227 (1926).

[27]C. P. Ho, J. D. Plummer, S. E. Hansen, and R. W. Dutton, IEEE Trans. Electron. Devices **ED-30**, 1438 (1983).

[28]S. Solmi, E. Landi, and F. Baruffaldi, J. Appl. Phys. **68**, 3250 (1990).

[29]F. A. Cotton and G. Wilkinson, *Advanced Inorganic Chemistry,* 5th ed. (Wiley, New York, 1988), Ch. 9.

[30]G. D. Watkins and J. W. Corbett, Phys. Rev. **121**, 1001 (1961).

[31]J. W. Corbett, G. D. Watkins, and R. S. MacDonald, Phys. Rev. **135**, A1381 (1964).

[32]R. Car, P. J. Kelly, A. Oshiyama, and S. T. Pantelides, Phys. Rev. Lett. **52**, 1814 (1984).

[33]W. Frank, in *Lattice Defects in Semiconductors,* edited by F. A. Huntley, IOP Conf. Proc. No. 23 (Institute of Physics and Physical Society, London, 1975), p. 23.

[34]K. Taniguchi, D. A. Antoniadis, and Y. Matushita, Appl. Phys. Lett. **42**, 961 (1983).

[35]T. Tsumuraya, S. A. Batcheller, and S. Masamune, Angew. Chem. Int. Ed. Engl. **30**, 902 (1991).

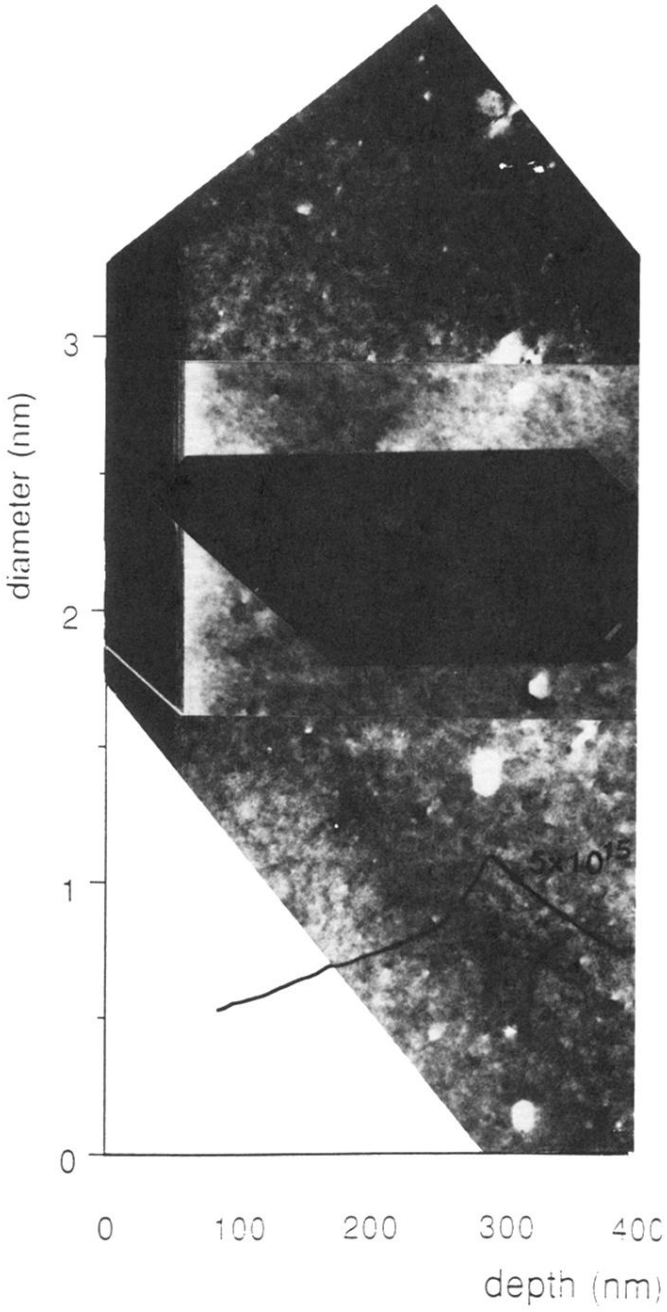

FIG. 10. Cross-section view of precipitates remaining after annealing at 1200 °C of the sample implanted at 5×10^{15} cm^{-2}, superimposed on the calculated diameter profile of precipitates produced in as-implanted conditions.

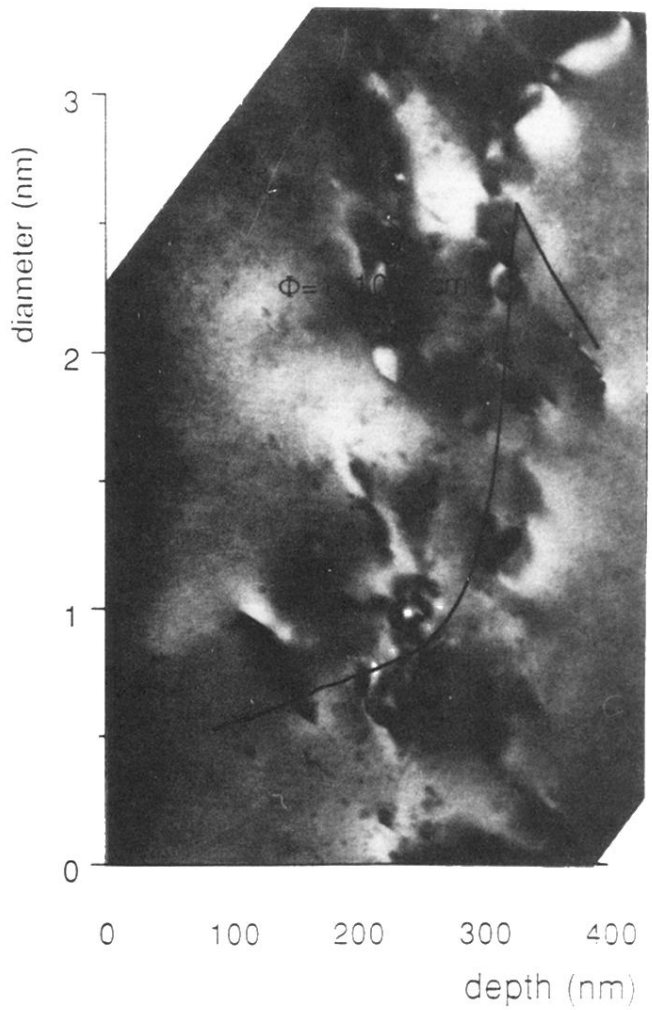

FIG. 13. Cross-section view of precipitates remaining after annealing at 1000 °C of the sample implanted at 1×10^{17} cm^{-2}, superimposed on the calculated diameter profile of precipitates produced in as-implanted conditions.

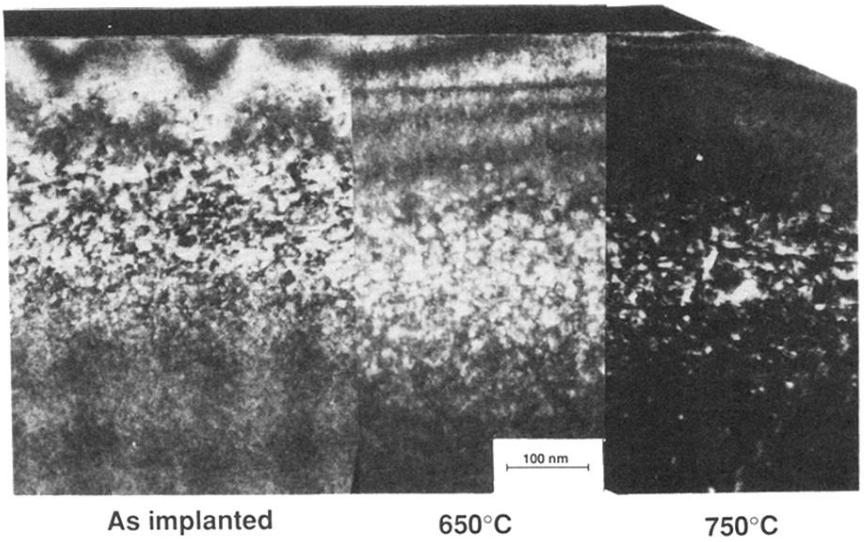

FIG. 4. Cross-section views of the implanted region in as-implanted and annealed samples; $\Phi = 5 \times 10^{15}\ \mathrm{cm}^{-2}$, $E = 100$ keV.

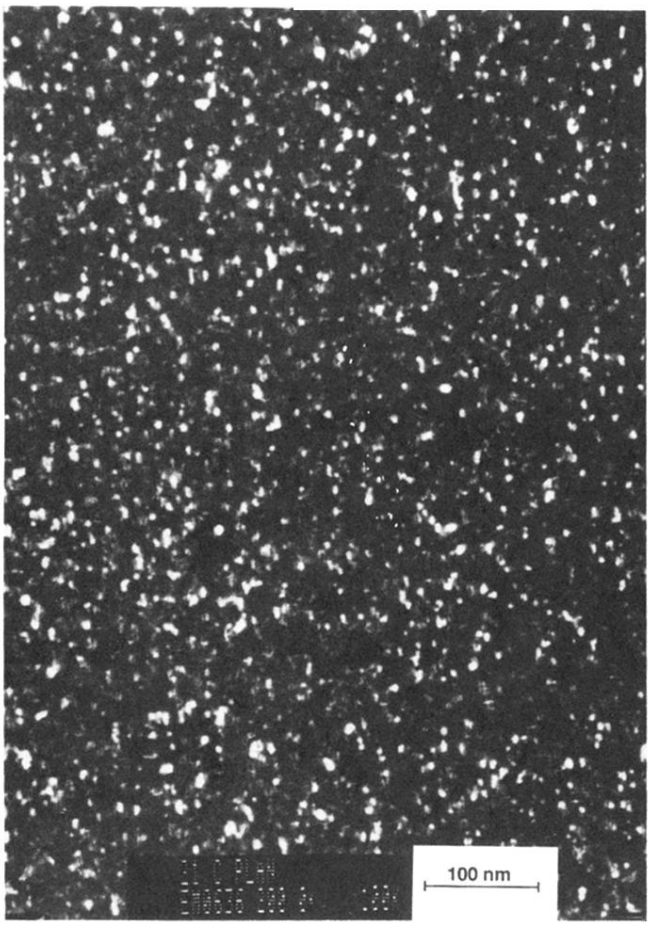

FIG. 5. Plan view of the implanted region in the sample implanted at $\Phi = 5 \times 10^{15}$ cm^{-2}, $E = 100$ keV and annealed at 650 °C.

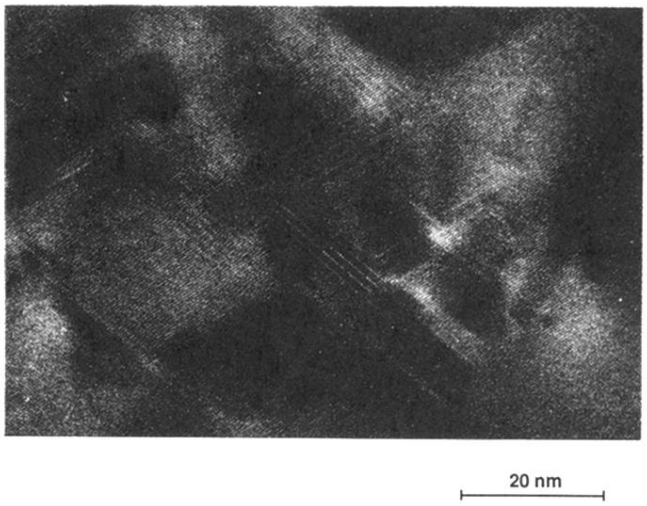

FIG. 6. High-resolution picture showing overlapping {111} stacking faults formed in the region of homogeneous precipitation after final annealing at 800 °C ($\Phi = 1 \times 10^{17}$ cm^{-2}, $E = 100$ keV).

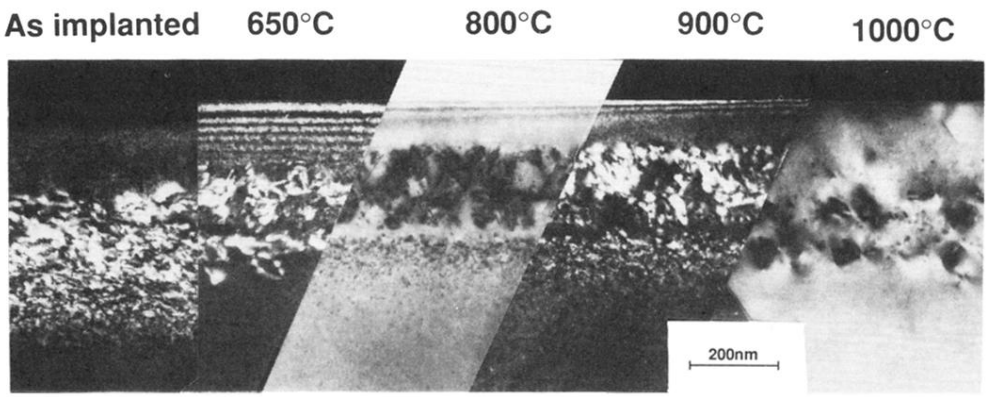

FIG. 7. Cross-section views of the implanted region in as-implanted and annealed samples; $\Phi = 1 \times 10^{17}$ cm^{-2}, $E = 100$ keV.